# Using Topo-Bathymetric Lidar to Map Eelgrass in Malpeque, PEI

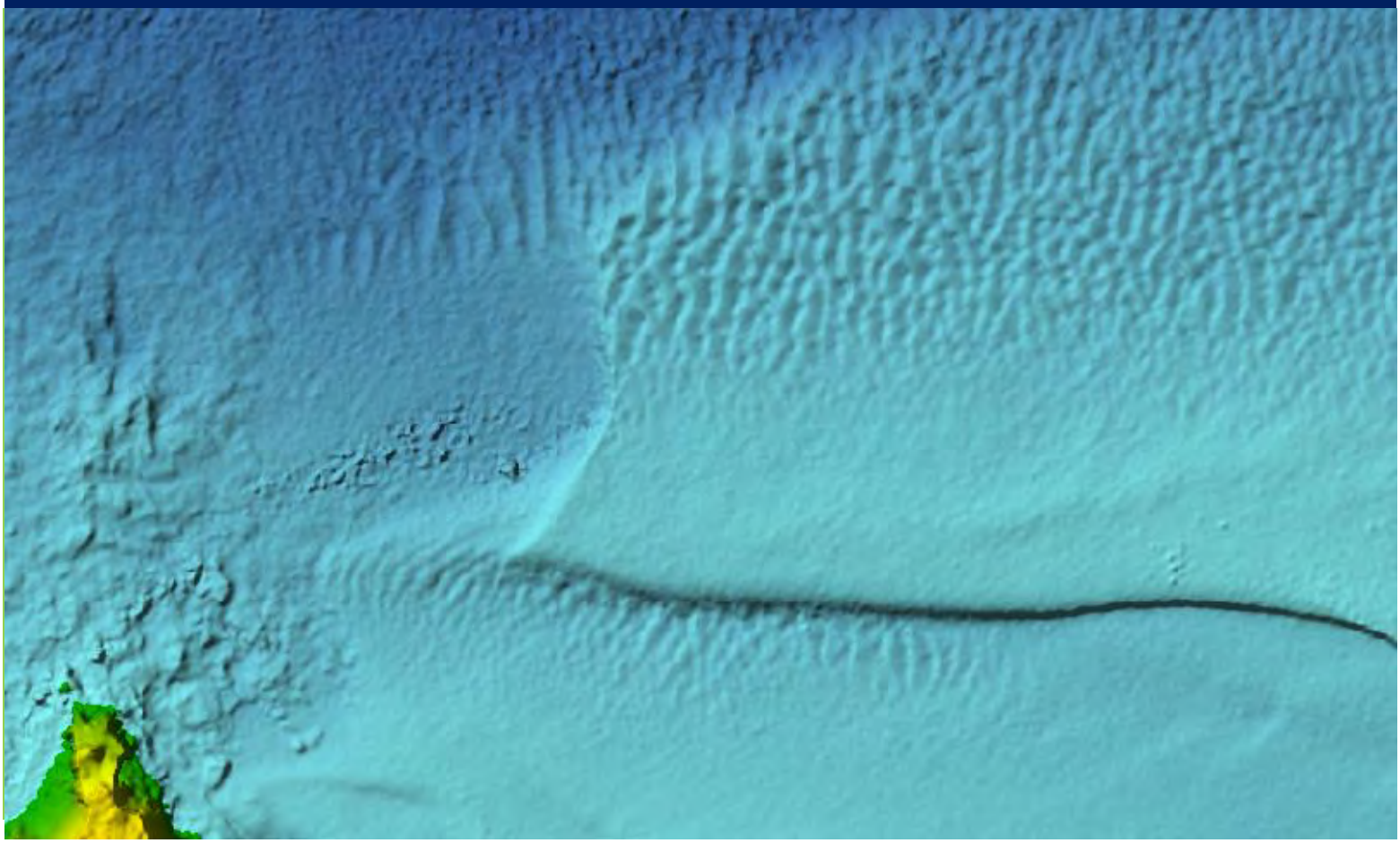


*Prepared by*

Applied Geomatics Research Group
NSCC, Middleton
Tel. 902 825 5475
email: tim.webster@nscc.ca

*Submitted to*

Taylor MacGregor
Engineer-in-Training
Englobe, Moncton
Tel. 5068572777


September 24, 2021

How to cite this work and report:

Webster, T., McGuigan, K., Crowell, N., Douglas, L. 2021. Using Topo-Bathymetric Lidar to Map Eelgrass in Malpeque, PEI. Technical report, Applied Geomatics Research Group, NSCC Middleton, NS.

Copyright and Acknowledgement

The Applied Geomatics Research Group of the Nova Scotia Community College maintains full ownership of all data collected by equipment owned by NSCC and agrees to provide the end user who commissions the data collection a license to use the data for the purpose they were collected for upon written consent by AGRG-NSCC. The end user may make unlimited copies of the data for internal use; derive products from the data, release graphics and hardcopy with the copyright acknowledgement of **"Data acquired and processed by the Applied Geomatics Research Group, NSCC"**. Data acquired using this technology and the intellectual property (IP) associated with processing these data are owned by AGRG/NSCC and data will not be shared without permission of AGRG/NSCC.

## Executive Summary

NSCC-AGRG surveyed the nearshore area of Malpeque Bay, PEI on July 29, 2021, and produced high resolution lidar and image data that were suitable for mapping coastal eelgrass. The results of this project demonstrate how topo-bathymetric lidar can be used to map underwater vegetation, even in areas that are sparsely vegetated. Eelgrass distribution was localised to the west of the dredged channel with minimal patches within the channel entry. The sensor collected data up to 9 m water depth but was unable to map the seafloor in the northwest section of the study site. While no data were collected in these deep waters, this did not inhibit NSCC-AGRG's mapping efforts as these areas were considered too deep to support the growth of eelgrass. Dark patches were mapped within sand ripples in the central portion of the study area around 6 m depth. While this depth could theoretically support eelgrass, DFO advised that even if eelgrass was present, it would be ephemeral and disturbed by natural causes in the depressions within the sand ripples. It may also be the case that these depressions are retaining dark material suspended within the water column. Data delivery consisted of an eelgrass location map, high-resolution lidar digital elevation model, depth normalized lidar intensity image, a lidar colour-shaded relief model, and a 0.05 m multispectral air photo mosaic.

## Table of Contents

# Table of Figures

# 1 Introduction

Eelgrass (*Zostera marina*) is the most dominant seagrass species in the northern hemisphere, and contributes to a wide range of ecosystem parameters, such as sediment stabilization, improvement of water clarity, and enhanced biodiversity (Olesen et al. 2015). In Canada, it is widespread on both the Pacific and Atlantic coasts, as well as the Hudson Bay (Environment and Climate Change Canada 2020). Seagrasses create one of the most productive yet highly threatened ecosystems on earth (van Katwijk et al. 2016). Global coverage of seagrass has been declining over the past century, with almost 30% of global coverage lost (Wong et al., 2013). Causes of decline have been attributed to anthropogenic influences, such as physical disturbances and changes in water parameters due to climate change.

Bathymetric lidar is an effective method for estimating water depth in coastal environments (Pan et al. 2016). Bathymetry data for shallow coastal waters is increasingly important to policy makers for science, resource management, and defense. It is considered vital to the management of disaster risk and toward guiding investment (Moffitt & Kumar 2018). Topo-bathymetric lidar also provides a tool to assess and map coastal and benthic habitat (Parrish et al. 2016). This method of seagrass mapping is cost effective and can cover a much larger area compared to traditional methods. The Nova Scotia Community College – Applied Geomatics Research Group (NSCC-AGRG) own and operate a Leica Chiroptera 4X (CH4X) high-resolution topo-bathymetric lidar scanner equipped with an ancillary Leica RCD30 60-megapixel multispectral (RGB-Nir) camera that can survey seabed morphology and habitat, including submerged vegetation (Webster et al., 2019). Malpeque Bay is actively dredged to allow for continued vessel passage. Sediment removed from the dredged area must be redeposited within a reasonable distance of the channel. Eelgrass maps produced by NSCC-AGRG will inform Englobe on potential areas where dredged sediment will not be detrimental to established eelgrass beds.

# 2 Methods

Methods on survey preparation, sensor management, and data processing are detailed in the following sections. Additional details can be requested from NSCC-AGRG if required.

## 2.1 Sensor Specifications and Installation

The lidar sensor used in this survey was the Leica Chiroptera 4X integrated topographic-bathymetric lidar sensor equipped with a 60-megapixel Leica RCD30 multispectral (RGB-Nir) camera. The lidar uses a 1064 nm near-infrared laser to survey ground and sea surface positions at 500 kHz and a green 515 nm laser to survey bathymetric positions at 35 kHz. The lasers scan in an elliptical pattern, which facilitates coverage from many different angles on vertical faces, produces fewer shadow effects in the data, and is less sensitive to wave interaction when compared to lateral ‘saw tooth’ scanners. The ability of the bathymetric laser to penetrate the water column is limited by water clarity. The system has a depth penetration rating of roughly 1.5 x visible extinction (Secchi depth). The Leica RCD30 camera collects coincident multispectral motion compensated imagery. NSCC-AGRG partnered with Leading Edge Geomatics (LEG) to charter a Piper

Navajo twin engine aircraft capable of housing the lidar unit. The CH4 was installed in the aircraft in Debert, NS on July 27, 2021, and calibrated on July 28, 2021, over a ground control site established by NSCC-AGRG in Truro.

## 2.2 Data Collection

Survey lines were planned using Leica Mission Pro at 400 m altitude at a speed of 65 m/s with 30% lateral overlap to ensure that no data gaps were present within the 0.6 km$^2$ area of interest (Figure 1). Data collection parameters supported a topo point density of >10 ppm, a bathy density of >5 ppm and aerial imagery with a ground pixel resolution of better than 5 cm. The Malpeque lidar survey was successfully completed on July 29, 2021, from 1300 to 1330 UTC. In-situ weather and GNSS constellation conditions were deemed suitable to support optimal data collection. Control for the survey was established by flying flat and level over two active control points proximal to the AOI in Ellerslie, PEI (PEEL 3533) and Gulf Shore, PEI (PEGS 3534). (Figure 2).

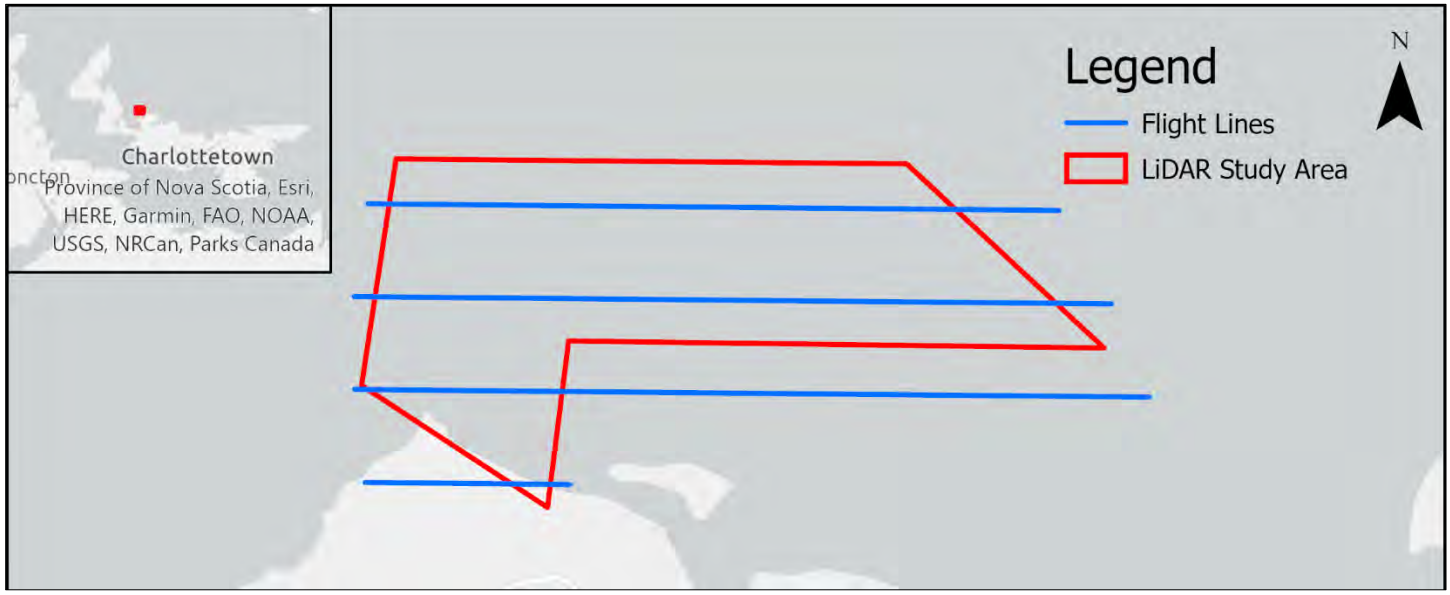


**Figure 1. Englobe study area and planned flight lines over Malpeque Bay, PEI.**


**Figure 2. Locations of the RTCM reference stations used during calibration flights for the LiDAR survey in Malpeque, PEI.**

## 2.3 Meteorological Condition Monitoring

Meteorological conditions during and prior to topo-bathy lidar data collection are an important factor in successful data quality because the bathy lidar sensor is limited by water clarity. Windy weather has the potential to stir up any fine sediment in the water and prevent good laser penetration, rain is not suitable for lidar collection, and sun angle can produce problematic glint in aerial imagery. Forecasted, current, and past weather conditions were monitored prior to data collection using the Summerside and Stanhope weather stations operated by Environment and Climate Change Canada (Figure 3). Conditions were deemed suitable to support optimal data collection at the time of survey.

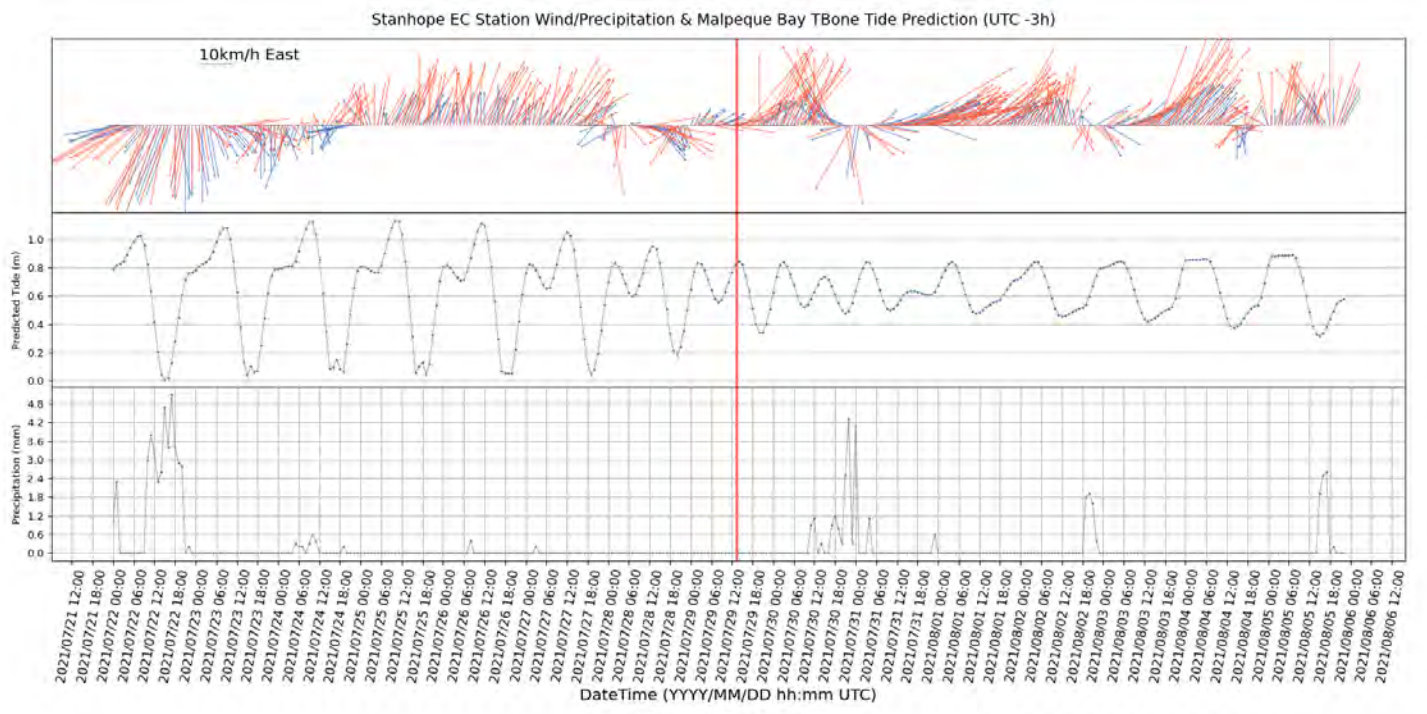


**Figure 3. Wind speed (km/h), precipitation (mm) and predicted tide (m) for the Malpeque Bay area. Wind data from the Stanhope EC weather station is plotted in blue, and the Summerside EC weather station is plotted in orange. Flight times are highlighted in red.**

## 2.4 Lidar Data Processing

A smoothed trajectory of the lidar and camera positions was calculated by linking system GNSS positions and IMU attitude with the control data from nearby stations using NovAtel Inertial Explorer. Leica Lidar Survey Studio (LSS) was used to process Chiroptera 4X waveforms to discrete georeferenced (NAD83 CSRSv7) points by linking laser returns to the processed aircraft trajectory to produce point clouds in the LAS format. The data were inspected to insure the AOI was fully surveyed. LAS files were read into Bentley TerraScan to analyze and further refine point metrics. Points were classified into discrete classes based on their physical characteristics including relative geometry and reflective properties (Table 1).

**Table 1. Lidar point classification values and descriptions**

| Classification Value | Meaning |
|---|---|
| 1 | Unclassified |
| 2 | Ground |
| 4 | Medium vegetation |
| 7 | Low point (noise) |
| 9 | Topographic water surface |
| 18 | High noise |
| 40 | Bathymetric point |
| 41 | Bathymetric water surface |
| 42 | Derived water surface |
| 80 | Bathymetric vegetation |

Two data products were derived directly from the lidar point cloud, 1) a rasterized digital elevation model (DEM) that included only returns that were classified as ground above and below the water line, and 2) a rasterized model of laser return intensities. Lidar return intensity is influenced by several factors including the local angle of incidence with the target, the natural reflectivity of the target material, the voltage or gain of the transmitted lidar pulse, and attenuation of the energy within the water column. Raw reflectance data are difficult to interpret due to these covariances and normalized values are needed to isolate the natural reflectivity of the target. A process has been developed to normalize the amplitude data for signal loss in a recent publication (Webster et al., 2016). The process involved sampling the amplitude data from a location with homogeneous seabed cover (e.g., sand or eelgrass) over a range of depths. These data were used to establish a relationship between depth and the logarithm of the amplitude value. The inverse of this relationship was used to adjust the amplitude data so that they could be interpreted without the bias of depth. A depth normalized amplitude/intensity raster (DNI) was created that can be used to interpret seabed cover material more consistently throughout the AOI. Note that this analysis considers only bathymetric lidar returns and ignores any topographic elevation points.

## 2.5 Image Processing

Multispectral RCD30 imagery was processed using Agisoft Metashape Professional. The processed smooth trajectory was linked to image events based on system time tags. This linkage was used to define the exterior orientation (EO) for each of the RCD30 images where camera position (x, y, z) and attitude (yaw, pitch, roll; omega, phi, kappa) were recorded for every exposure with positional accuracies better than 0.01 m and rotational accuracies better than 0.004 degrees. Any ambiguity between relief displacement and lens distortion was solved using by generating a well-defined internal orientation (IO) of the engineered zero distortion RCD30 lens and CCD during the camera boresight process at the Truro calibration site. Captured imagery was positioned using an aerial triangulation model where possible to generate the best relief map for subsequent orthorectification. Where photo positions were unable to be resolved, such as deep open water with few image tie-points, imagery was directly georeferenced using the EO and IO. In both cases imagery was georeferenced to within 5 cm.

## 2.6 Submerged Aquatic Vegetation Mapping

Submerged Aquatic Vegetation (SAV) has been successfully mapped in several CH4X data collections by combining aerial imagery, normalized lidar reflectance values, and accurate depth models derived from lidar (Figure 4). In relatively clear water conditions this technique can produce a clear image of SAV. The SAV prediction logic is based on the understanding that vegetation absorbs more energy, and appear darker, relative to surrounding sands. This interaction becomes apparent when depth normalization and has been applied to the lidar (Figure 5) and imagery (Figure 6). The image derived product was computed using a normalized difference technique which included red, green, and blue image values. As with the lidar, image radiometric signatures were normalized by depth using the lidar depth model described in the equation below:

$$\mathrm{SAV}_{RGB} = \left[\frac{Red - Green}{Red + Green} + \frac{Green - Blue}{Green + Blue} + 0.1\right] * \frac{1}{0.2}$$

$$\mathrm{SAV}_{515nm} = [-6.8\,] * \frac{1}{4.3}$$

$$\mathrm{DS}_{depth} = depth * \frac{1}{-6.5}$$

Many band ratios in the visible light spectrum illustrate a linear relationship with respect to water depth while lidar reflectance exhibits an exponential rate of decay. Therefore, the relationship of the natural logarithm of the lidar reflectance to depth is linear. Each image derivative was appropriately scaled such that the resulting range would align with the lidar depth image from 0 m up to a maximum depth of 6.5 m such that the linear depth compensation could be performed directly.

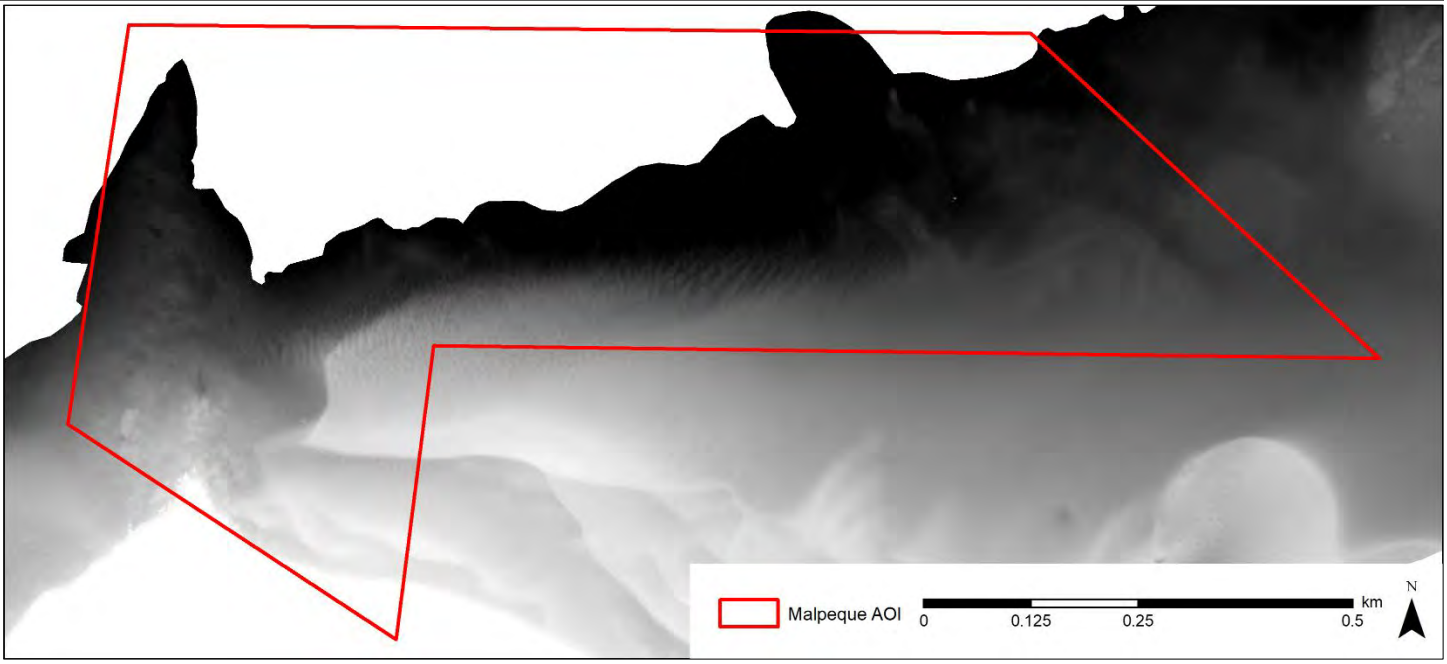


**Figure 4. Lidar depth map showing a gradient of water depths from 0 m (white) to 9 m depth (black).**

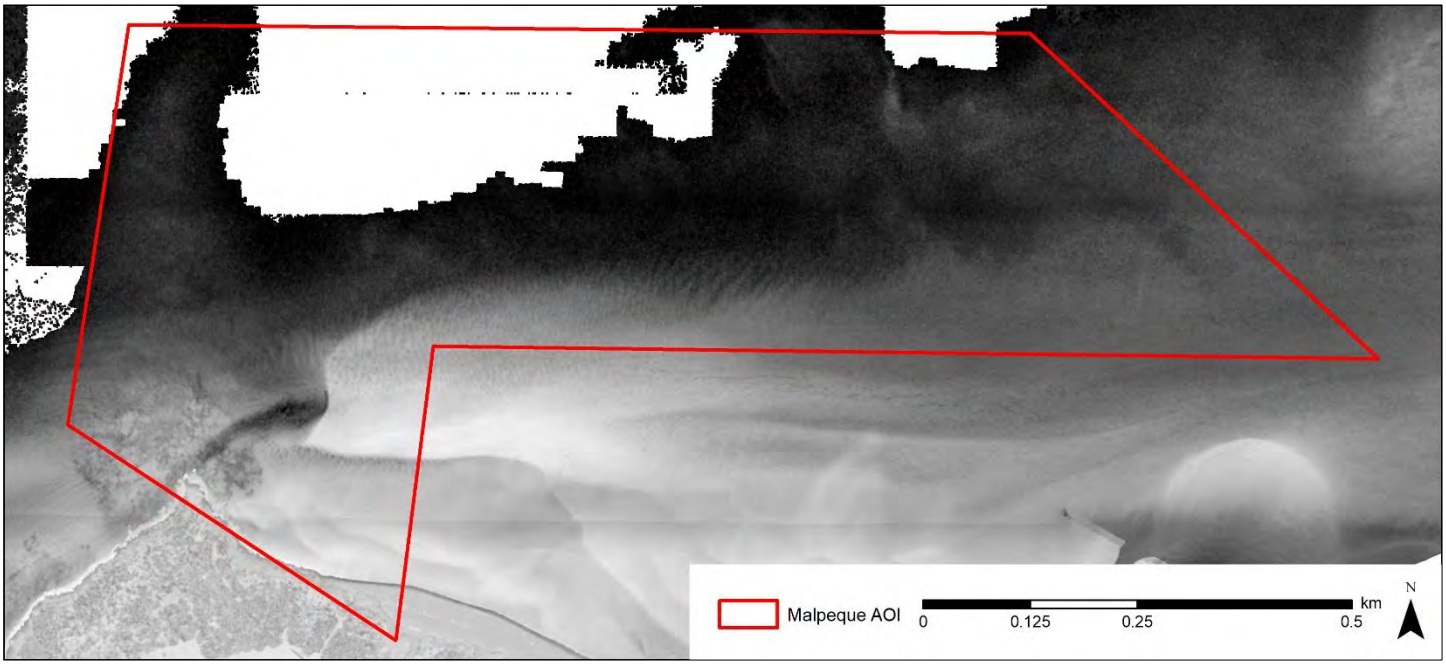


**Figure 5. Lidar intensity map which separates less reflective materials, like eelgrass (dark), from highly reflective materials, such as sand (bright).**

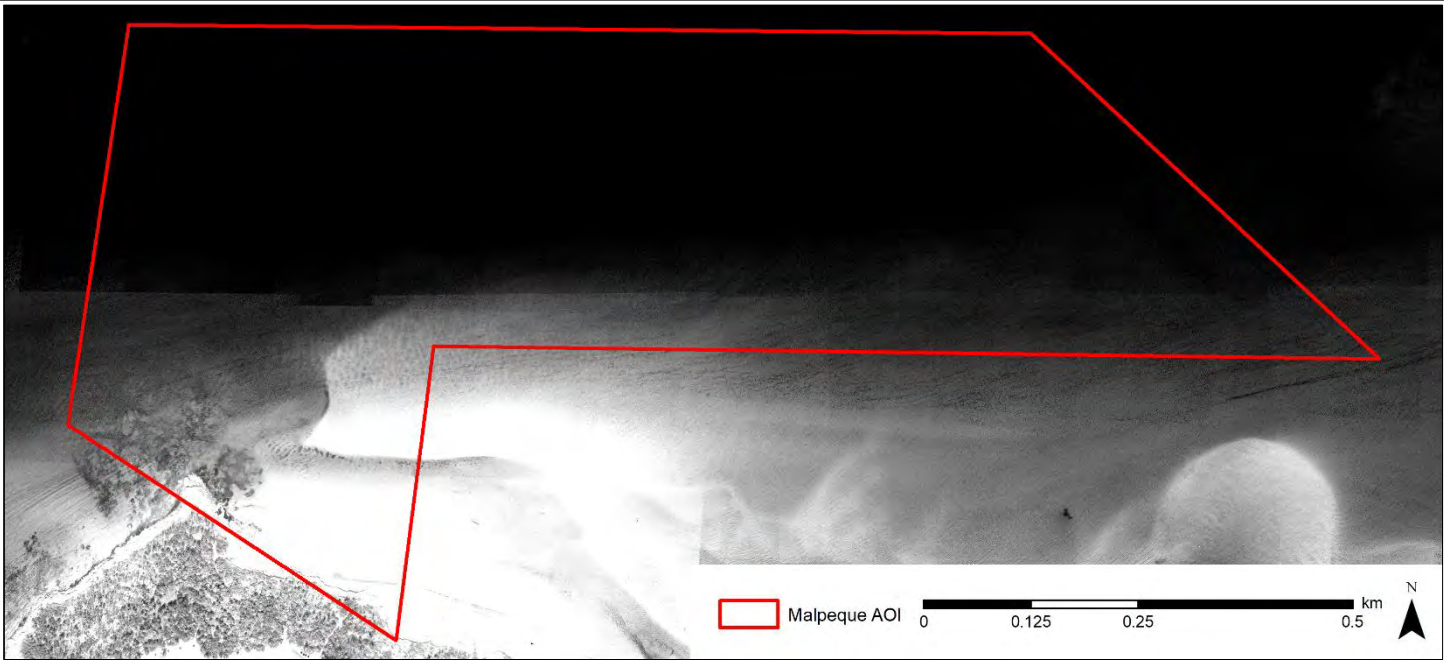


**Figure 6. RCD30 derived normalized difference map which minimizes wave and glint artifacts while separating dark eelgrass from sand. This technique breaks down in deeper water in the north of the AOI.**

A principal reason for building SAV indexes for each sensor is that they each have various benefits and limitations. The SAV model derived from the camera sensor performed better in very shallow waters, less than 1 m depth, where the lidar reflectance is susceptible to peaking and exhibiting noise due to complex water surface interactions. The lidar shows a stronger sea floor reflectance up to a much greater depth (>7 m) compared to the camera. Both sensors have various technical artifacts which can diminish the result of their individual SAV products including sea surface glint, sediment plumes, water characteristics, signal loss due to incident angle, and changing light conditions. These problems are inconsistent between the sensors and a fusion of their SAV products helps to produce a superior model. Various approaches have been experimented with to amalgamate these models and based on the extent of the various technical aspects which affect each sensor the maximum returning value from both models was used to map SAV in the Malpeque AOI (Figure 7):

$$SAV_{index} = \max\left[\left(\mathrm{SAV}_{RGB} + \mathrm{DS}_{depth}\right), \left(\mathrm{SAV}_{515nm} + \mathrm{DS}_{depth}\right)\right]$$


**Figure 7. Eelgrass confidence map generated using the image based SAV map, the lidar based SAV map, and depth. Eelgrass appears darker than surrounding bottom materials with little inconsistency.**

The resulting raster represented a vegetation presence index which was further refined by a thresholding procedure to generate a binary result where a value of 1 was representative of SAV presence and a value of 0 was representative of SAV absence:

$$SAV_{presence} = SAV_{index} < 0.95$$

## 3 Results

The AOI was over-collected to ensure the area was fully scanned by the CH4X. The total area scanned was approximately 3 km$^2$ while the study area was 0.6 km$^2$. All products met or exceeded project goals. Topo lidar was collected at a density of >10 ppm, bathymetric lidar was collected at a density of >5 ppm to a depth of >9 m and imagery was collected at a native resolution of 0.046 m. There were no gaps in coverage, though extinction of the bathymetric signal did occur in the northern section of the AOI. Both the laser and image products were suitable for generating an eelgrass map and several additional deliverables discussed within the following section. For delivery, map data have been projected to the Universal Transverse Mercator Zone 20 North, following the North American Datum of 1983 Canadian Spatial Reference System Version 7 horizontal coordinate system, and the Canadian Geodetic Vertical Datum of 2013 vertical coordinate system (prjUTM20N_hcsNAD83CSRSv7_vcsCGVD2013)

## 3.1 Image Products

The orthophoto mosaic product was generated at a resolution of 0.05 m resolution with pixel perfect alignment between frames and covered the entire extent of the AOI (Figure 8). The quality of the imagery was suitable for assisting with the interpretation of the DEM and eelgrass coverage though context-based contrast and brightness enhancements (Figure 9).


**Figure 8. True colour orthomosaic of Malpeque Bay, PEI created using Agisoft Metashape Professional 1.7.2.**

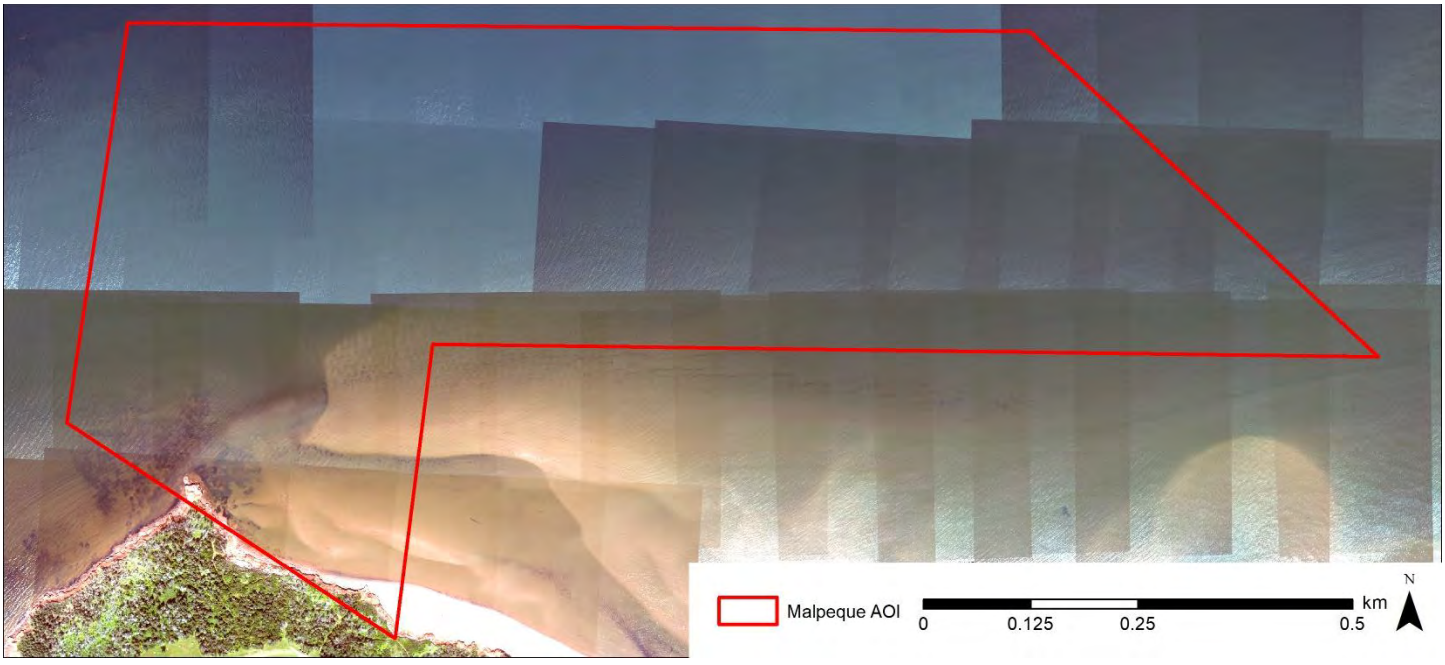


**Figure 9. Enhanced imagery provides more detail on vegetation coverage while producing additional image artifacts between frames. This type of enhancement is suitable for visual inspection, but models poorly.**

## 3.2 Lidar Products

The bathy lidar penetrated to roughly 9 m depth but was unable to map the seafloor in the northwest section of the study site. While no data were collected in these deep waters, this did not inhibit NSCC-AGRG's mapping efforts as these areas were considered too deep to support the growth of eelgrass. Topographic and bathymetric data were of high quality and exhibited very little noise which resulted in smooth elevation models (Figure 10) and colour shaded relief models that combine elevation information from the DEM with a colour ramp to highlight differences in elevation (Figure 11).

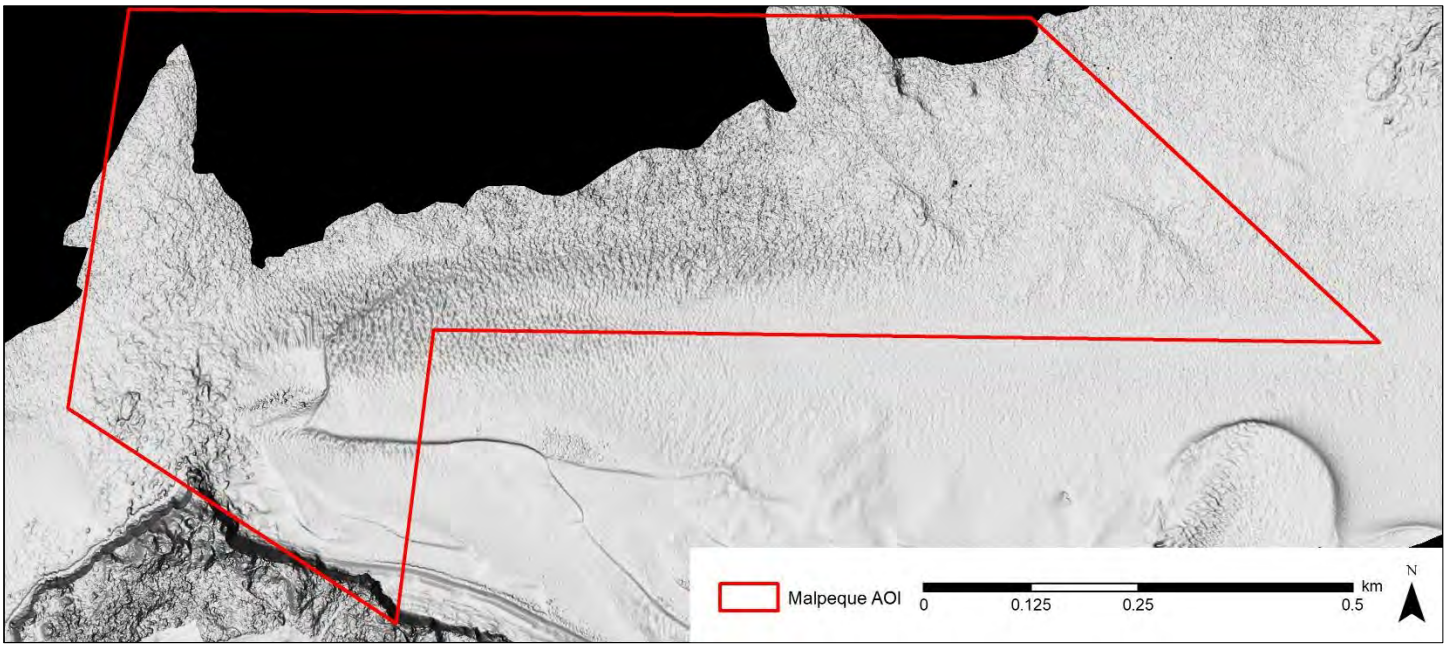


**Figure 10. Seamless topo-bathy digital elevation model of Malpeque Bay, PEI with 5 times vertical exaggeration.**

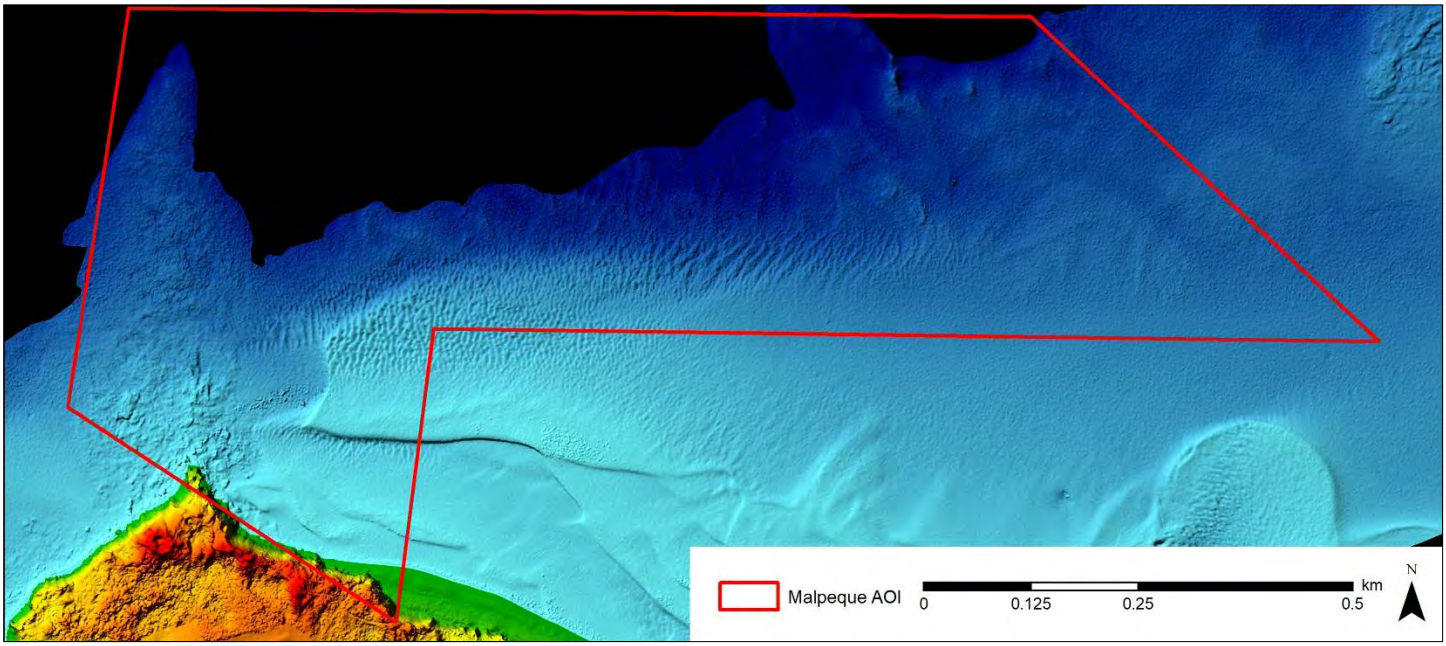


**Figure 11. Colour shaded relief model of the study area in Malpeque Bay, PEI. The DEM CSR shows the separation of land and water at 0 m CGVD2013 at the blue-green boundary.**

The normalized bathymetric intensity model compensated for the variation in depth in Malpeque Bay and the impact on the amplitude of the reflected green laser pulses (Figure 12). Depth contour maps were generated for the highly dynamic area proximal to the dredged channel that further highlight variations in depth (Figure 13).

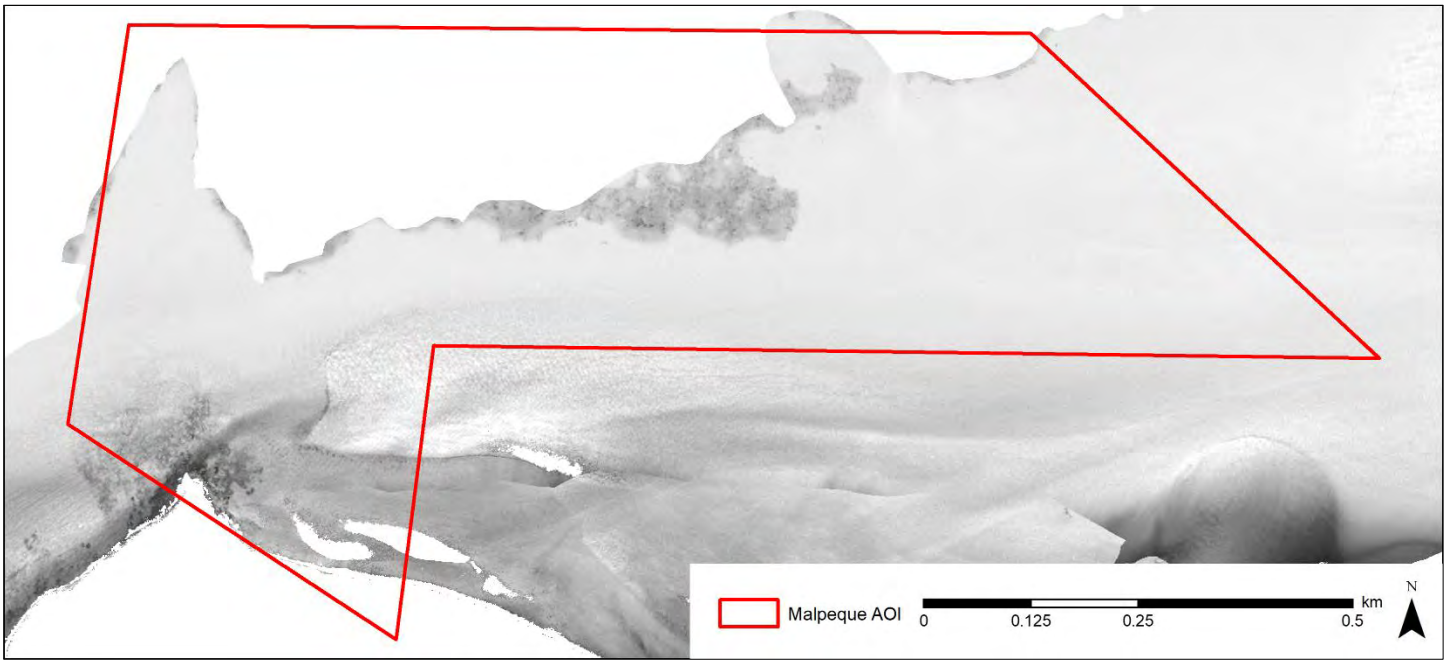


**Figure 12. Depth normalized intensity map which separates highly absorbent materials, like eelgrass, from highly reflective materials, such as sand, regardless of depth.**

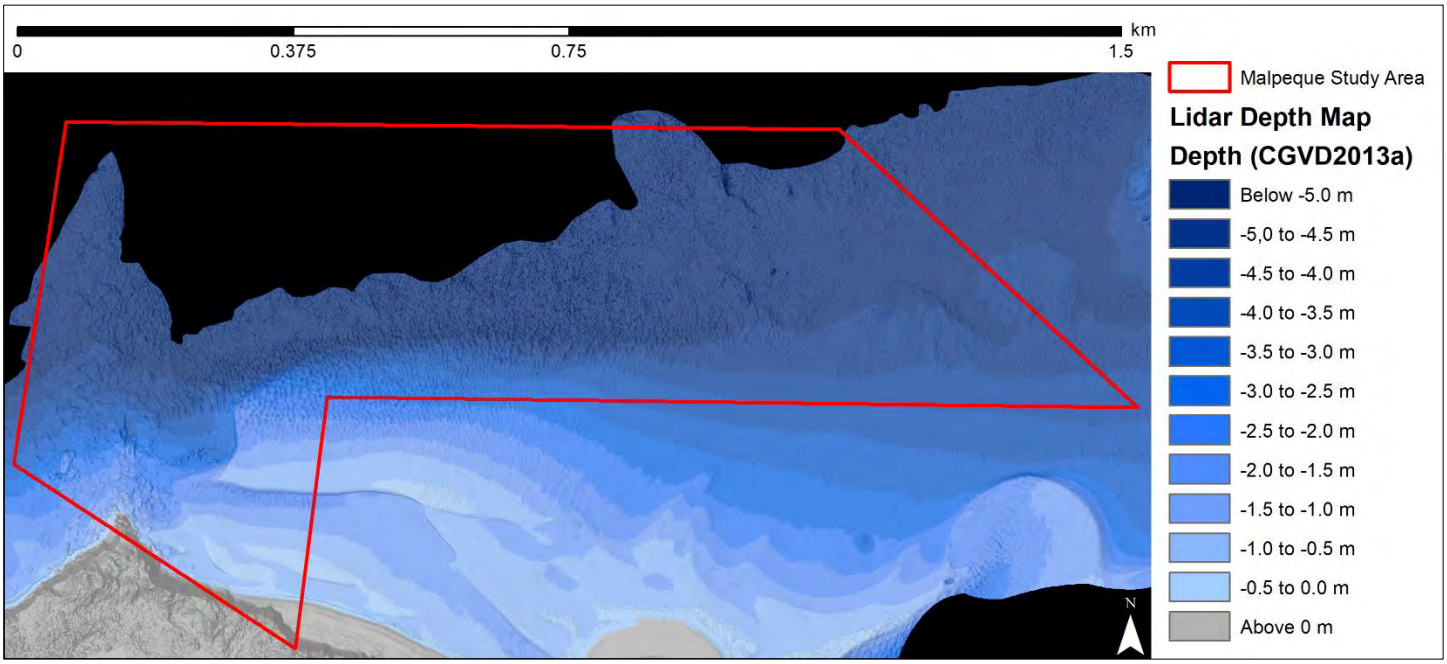


**Figure 13. Depth contour map showing depth contours every 0.5 m in Malpeque Bay, PEI.**

## 3.3 Submerged Aquatic Vegetation Map

Eelgrass and other seagrasses were successfully mapped and were found to be most prominent around the cape to the west of the dredged channel with few patches on the south and west bank of the migrating sand at the end of the channel (Figure 14). These areas are important to note, as Englobe client wishes to avoid areas with eelgrass for dredge dumping.

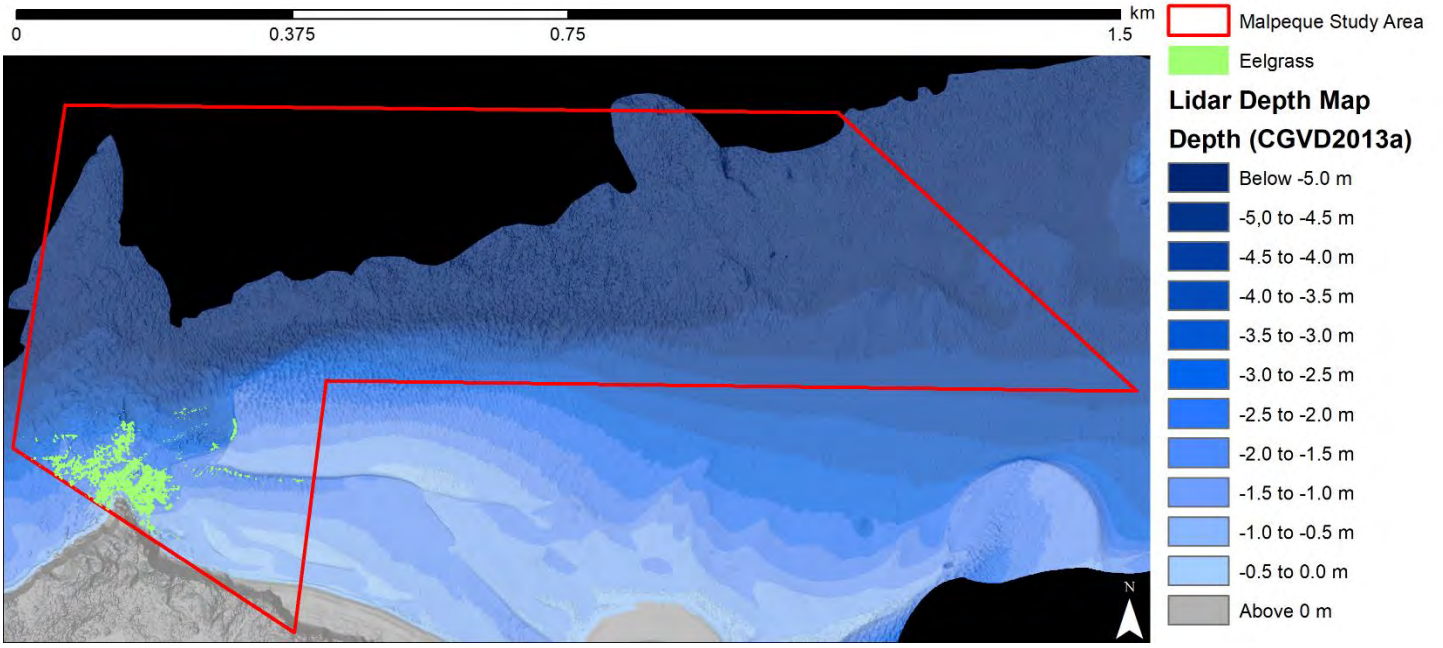


**Figure 14. Submerged aquatic vegetation presence absence map with a threshold set to display high confidence eelgrass location within the Malpeque Bay, PEI study area.**

# 4 Discussion

Three separate approaches were examined for mapping eelgrass and other seagrasses in the Malpeque Bay area: a localized roughness approach, a lidar reflectance approach, and a multispectral imagery approach. Each method had benefits and unique challenges. For this area, the roughness technique was not incorporated as it generally produced an inconsistent final product. Image band-ratio composites successfully indicated dark seafloor features such as vegetation while reducing the impact of sun angle and water surface. The lidar reflectance approach was valuable as the green laser penetrated deeper in the water than any of the camera bands.

Malpeque Bay is a high energy area that has constantly changing bottom features which invalidate the use of historical imagery to validate data. In such high energy areas, storms can cause significant seagrass loss (Côté-Laurin et al. 2017, Oprandi et al. 2020). Eelgrass distribution and abundance may have changed between the most recent satellite imagery and the lidar survey for this project. Seagrasses can take years to recover from disturbance (O'Brien et al. 2018) and multiple disturbances over many years could cause significant decline in eelgrass in this area. It will be important to create up to date eelgrass maps for the Malpeque Bay area if continued dredging is being considered. Large areas of shifting sand can appear similar in reflectance to vegetation resulting in an overestimation of eelgrass presence. This is specifically an issue in the Malpeque area, recent aerial photography indicates the sand bar within this area of interest has continued to shift significantly (Figure 15). Dark patches were mapped within sand ripples in the central portion of the study area around 6 m depth. While this depth could theoretically support eelgrass, DFO advised that even if eelgrass was present, it would be ephemeral and disturbed by natural causes in the depressions within the sand ripples.

Composite imagery highlights the variation between the RCD30 camera and the lidar reflectance with respect to depth (Figure 16). Blue features are those which are shallow and dark with respect to the RCD30 and lidar reflectance while. These areas are interpreted as submerged vegetation. The strong and smooth red patterns trending west to east across the scene indicate areas of high RCD30 reflectance with strong absorption in the lidar laser and can be interpreted as particulate in the water column. Sand ripples observed at greater depth suggests vegetation may be present, however this cannot be clearly determined from the reflectance of either sensor.

**Figure 15. (From top to bottom) Google Earth images of Malpeque Bay, PEI show a shifting sand from August 6, 2012, April 17, 2014, July 22, 2017, July 10, 2019, and May 30, 2021, with the AOI study area outlined in red.**


**Figure 16. Composite imagery generated using each component used to derive the SAV model show complex patterns of suspended material, submerged vegetation, and sand ripples; RCD30 imager derivative (red) lidar reflectance (green) and depth (blue).**

# 5 Conclusion

NSCC-AGRG surveyed the nearshore area in Malpeque Bay, PEI on July 29, 2021, and produced high resolution lidar and image data suitable for mapping coastal eelgrass. The results of this project demonstrate how topo-bathymetric lidar can be used to map underwater vegetation even in areas that are sparsely vegetated.

This project has demonstrated the multiple uses of data derived from a single topo-bathymetric lidar survey to support eelgrass conservation efforts. Several key datasets were derived from the lidar seamless land-sea elevation data including the digital elevation model (DEM), the depth normalized intensity (DNI) model, the colour shaded relief (CSR), and the depth contour map with seagrass presence. The methods developed in this project can be used to monitor changes in eelgrass distribution in Malpeque Bay and map eelgrass beds elsewhere. As seagrasses worldwide are highly threatened (van Katwijk et al. 2016), it is more important than ever to have monitoring procedures in place.

# 6 Acknowledgements

We like to thank Jeff Barrelhead of DFO for providing expert advice on eelgrass distribution characteristics. Thanks to staff from Leica Airborne Hydrography and Leica Geosystems for operational support, Leading Edge Geomatics for their flexible hours and piloting skills, and additional NSCC staff for administrative support and data processing efforts.

# 7 References

Côté-Laurin, M. C., Benbow, S., & Erzini, K. (2017). The short-term impacts of a cyclone on seagrass communities in Southwest Madagascar. *Continental Shelf Research* 138: 132-141.

Environment and Climate Change Canada (2020) Canadian Environmental Sustainability Indicators: Eelgrass in Canada. Consulted on *September 2, 2021*. Available at: www.canada.ca/en/environment-climate-change/services/environmental-indicators/eelgrass-canada.html.

Moffitt, D.L. and Kumar, L. (2018). Remote sensing of a shallow, fringing reef platform for analysis of island sector susceptibility and development of a coastal vulnerability index. *Journal of Coastal Research* 34(1): 122–135.

NatureServe. 2019. NatureServe Explorer: An online encyclopedia of life [web application]. Version 7.1. NatureServe, Arlington, VA. Web site: http://explorer.natureserve.org [Accessed August 2021].

O'Brien, Katherine R., Michelle Waycott, Paul Maxwell, Gary A. Kendrick, James W. Udy, Angus JP Ferguson, Kieryn Kilminster et al (2018). Seagrass ecosystem trajectory depends on the relative timescales of resistance, recovery and disturbance. *Marine pollution bulletin* 134: 166-176.

Olesen, Birgit, Dorte Krause-Jensen, Núria Marbà, and Peter Bondo Christensen (2015). Eelgrass Zostera Marina in Subarctic Greenland: Dense Meadows with Slow Biomass Turnover in Cold Waters. *Marine Ecology Progress Series* 518: 107-21.

Oprandi, A., L. Mucerino, F. De Leo, C. N. Bianchi, C. Morri, A. Azzola, F. Benelli, G. Besio, M. Ferrari, and M. Montefalcone (2020). Effects of a severe storm on seagrass meadows. *Science of the Total Environment* 748: 141373.

Pan, Z., Glennie, C., Fernandez-Diaz, J. C., & Starek, M. (2016). Comparison of bathymetry and seagrass mapping with hyperspectral imagery and airborne bathymetric LiDAR in a shallow estuarine environment. *International Journal of Remote Sensing* 37(3): 516-536.

Parrish, C.E.; Dijkstra, J. A.; O 'Neil-Dunne, J.P.M; McKenna, L., and Pe'eri, S. (2016). Post-Sandy benthic mapping using new topobathymetric LiDAR technology and object-based image classification. In: Brock, D.B.; Parrish, C.E.; Rogers, J.N., and Wright, C.W. (eds.), Advances in Topobathymetric Mapping, Applications. Jo*urnal of Coastal Research , Special Issue* 76: 200-208.

van Katwijk, M. M., Thorhaug, A., Marbà, N., Orth, R. J., Duarte, C. M., Kendrick, G. A., ... & Verduin, J. J. (2016). Global analysis of seagrass restoration: the importance of large-scale planting. *Journal of Applied Ecology* 53(2): 567-578.

Webster, T., McGuigan, K., Crowell, N., Collins, K. and Lauzon-Guay, J.S. (2019). Calculating macroalgal height and biomass using bathymetric LiDAR and a comparison with surface area derived from satellite data in Nova Scotia, Canada. Botanica Marina 10.1515/bot-2018-0080, on-line. https://www.degruyter.com/document/doi/10.1515/bot-2018-0080/html

Webster, T., McGuigan, K., Crowell, N., Collins, K. and MacDonald, C. (2016). Optimization of data collection and refinement of post-processing techniques for Maritime Canada's first shallow water topographic-bathymetric LiDAR survey. Journal of Coastal Research. Special issue on Advances in Topo-Bathymetric LiDAR. Vol 76: pp. 31-43.

Wong, Melisa C., Monica A. Bravo, and Michael Dowd. (2013). Ecological dynamics of Zostera marina (eelgrass) in three adjacent bays in Atlantic Canada. *Botanica Marina* 56(5-6): 413-424.